doi:10.1038/nature11776

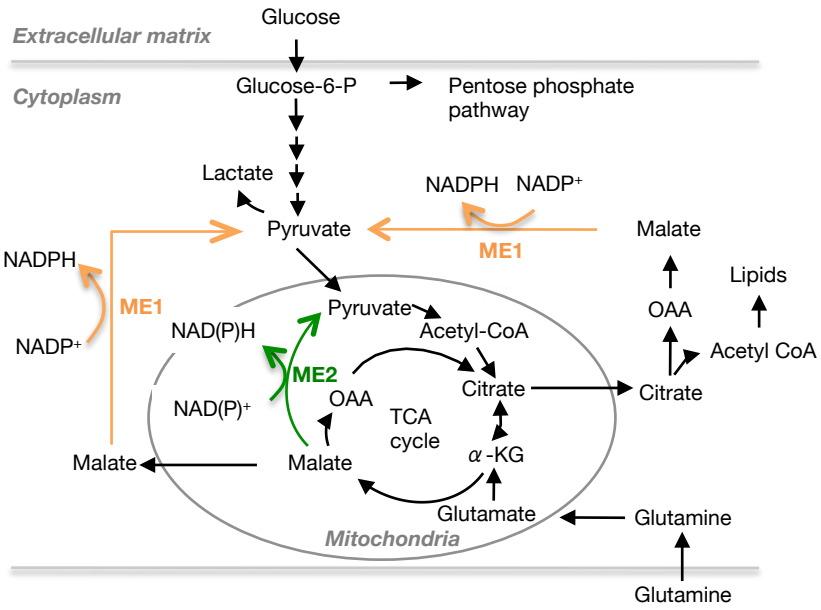

Supplementary Figure 1 | The metabolic pathways involving ME1 and ME2. The cytoplasmic and mitochondrial MEs convert malate to pyruvate and generate either NADPH or NADH. They are generally thought to adjust the TCA flux under different nutritional and growth conditions. OAA, oxaloacetate; α-KG, α-ketoglutarate.

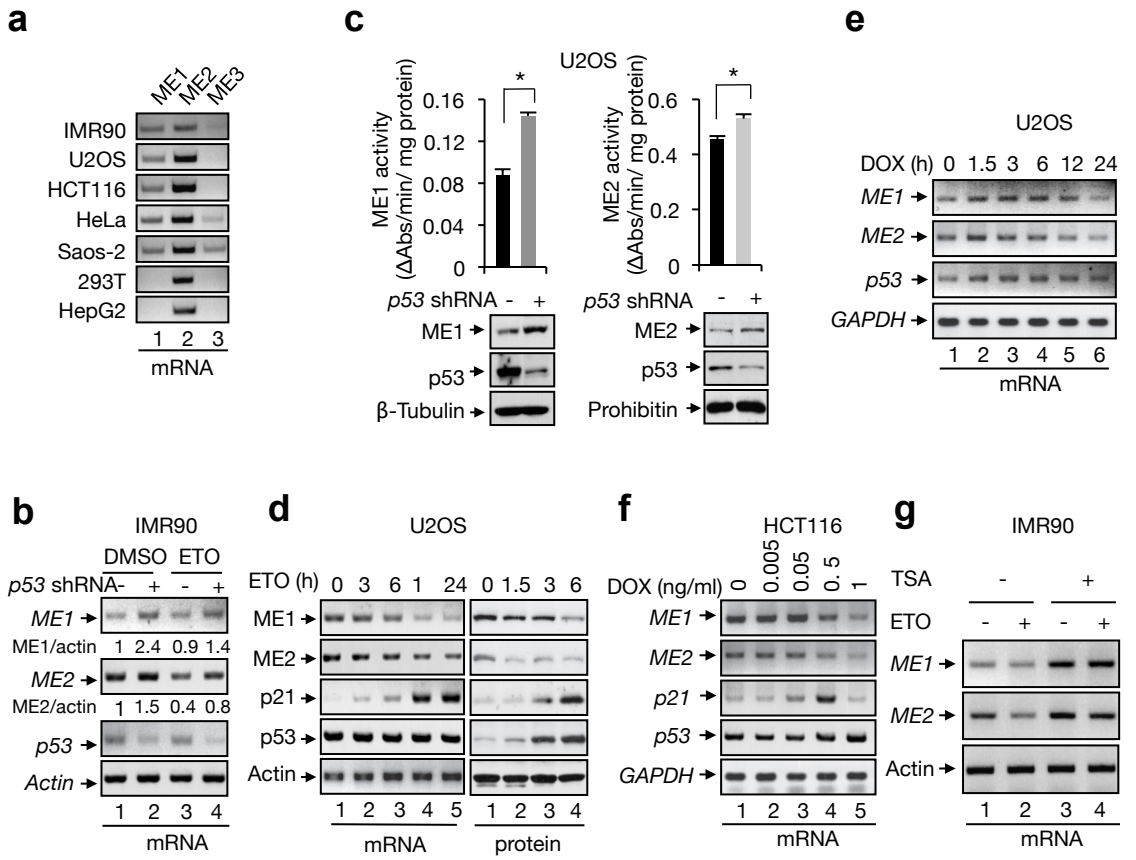

Supplementary Figure 2 | *ME1* and *ME2* are p53 target genes. a, Expression of ME1, ME2, and ME3 in different cell lines was compared using RT-PCR. **b**, IMR90 cells stably expressing *p53* shRNA or control shRNA were treated with or without ETO (20 μM). Expression of ME1, ME2, p53, and, as a control, Actin, were analyzed by RT-PCR. The relative ratios of ME1 and ME2 to actin are shown. **c**, ME1 and ME2 activity in U2OS cells stably expressing *p53* shRNA or control shRNA (means ± SD, n=3). Protein expression is shown below. **d**, U2OS cells were treated with ETO (20 μM). The expression of ME1, ME2, p53, and the p53 target gene *p21* was detected using RT-PCR (left) and western blot (right). **e**, U2OS cells treated with 1 μg/ml doxorubicin (DOX) for the indicated durations were analyzed for the mRNA levels of ME1, ME2, p53, and, as a control, GAPDH by RT-PCR. **f**, $p53^{+/+}$ HCT116 cells were treated with increasing amounts of DOX for 24 hours, and the expression of ME1, ME2, p21, and p53 was analyzed by RT-PCR. **g**, IMR90 cells were treated with ETO (20 μM) and TSA (100 nM) as indicated for 24 h. The expression of ME1 and ME2 was detected using RT-PCR.

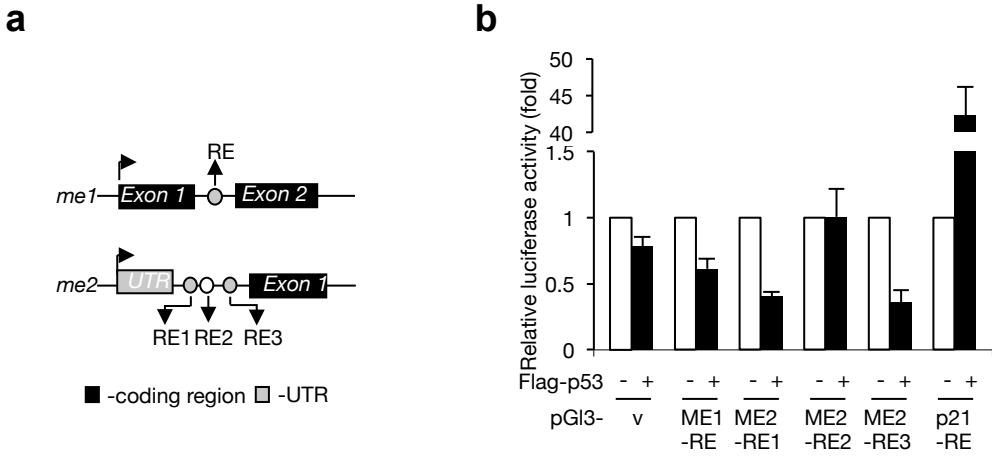

Supplementary Figure 3 | Direct repression of *ME1* and *ME2* genes by p53. **a**, The genomic structure of human *ME1* and *ME2*. Shown are the exon/intron organization, a potential p53 response element (ME1-RE) within the first intron of the ME1 gene, and three potential p53 REs within the first intron of the *ME2* gene (ME2-RE1, -RE2, and -RE3). See Supporting Online Material for the RE sequences. **b**, Promoter reporter assay with ME1- or ME2-RE constructs in 293T cells co-transfected with or without the p53 expression vector (means ± standard deviation (SD); n=3).

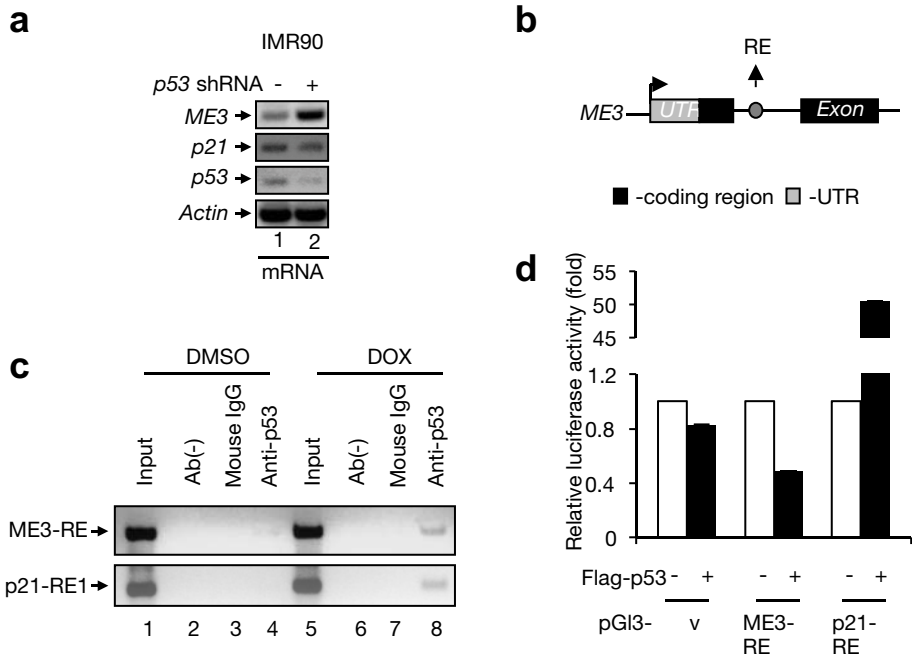

Supplementary Figure 4 | Suppression of ME3 expression by p53. a, IMR90 cells stably expressing *p53* shRNA or control shRNA were assayed for the expression of ME3, p21, and p53 by RT-PCR. **b**, The genomic structure of human *ME3*. Shown are the exon/intron organization and a potential p53 response element within the first intron. **c**, $p53^{+/+}$ HCT116 cells treated with or without DOX (1 μg/ml) for 24 h were subjected to ChIP with anti-p53 (DO-1), a control mouse IgG, or no antibody (-). **d**, 293T cells were co-transfected with ME3- or p21-RE constructs with or without the p53 expression vector (means ± SD, n=3).

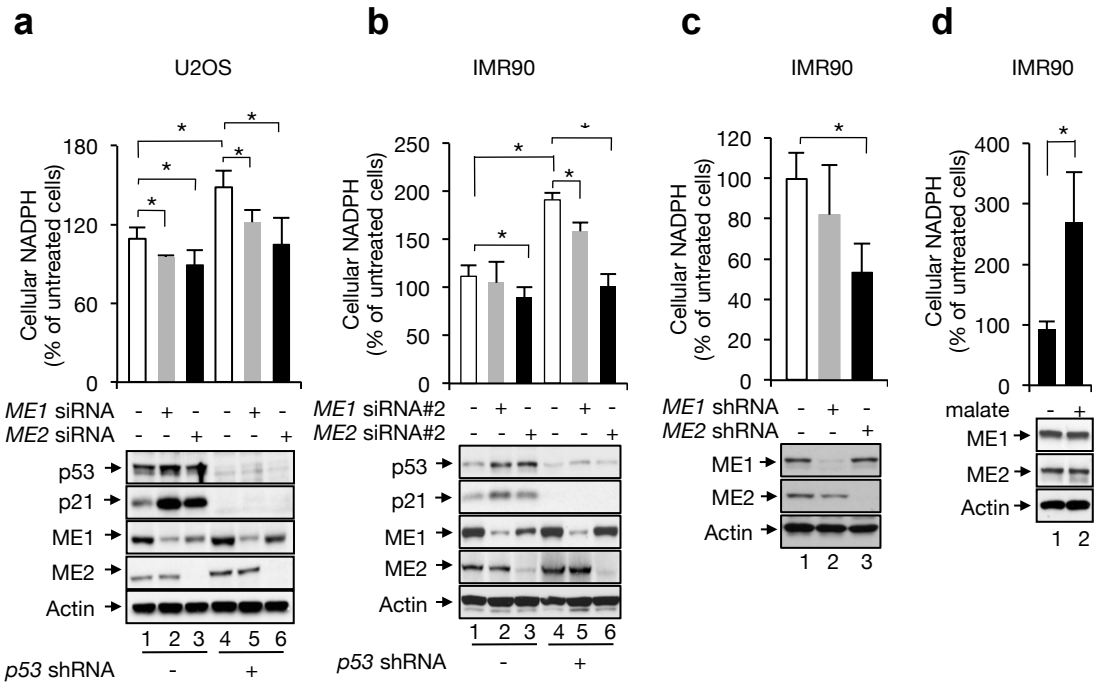

Supplementary Figure 5 | Role of ME1 and ME2 in NADPH production. a, U2OS cells stably expressing *p53* shRNA or control shRNA were treated with *ME1* or *ME2* siRNA as indicated. NADPH levels (means ± SD, n=3; top) and protein expression (bottom) are shown. **b**, IMR90 cells stably expressing *p53* shRNA or control shRNA were treated with *ME1* or *ME2* siRNA that was different from those used in **a** and Fig. 2a. NADPH levels (means ± SD, n=3; top) and protein expression (bottom) are shown. **c,** IMR90 cells stably expressing *ME1*, *ME2* or control shRNA were assayed for NADPH levels (top) and protein expression (bottom). **d,** IMR90 cells treated with or without a membrane permeable form of malate (dimethyl L-malate) for 24 h were assayed for NADPH levels (means ± SD, n=3; top) and protein expression (bottom).

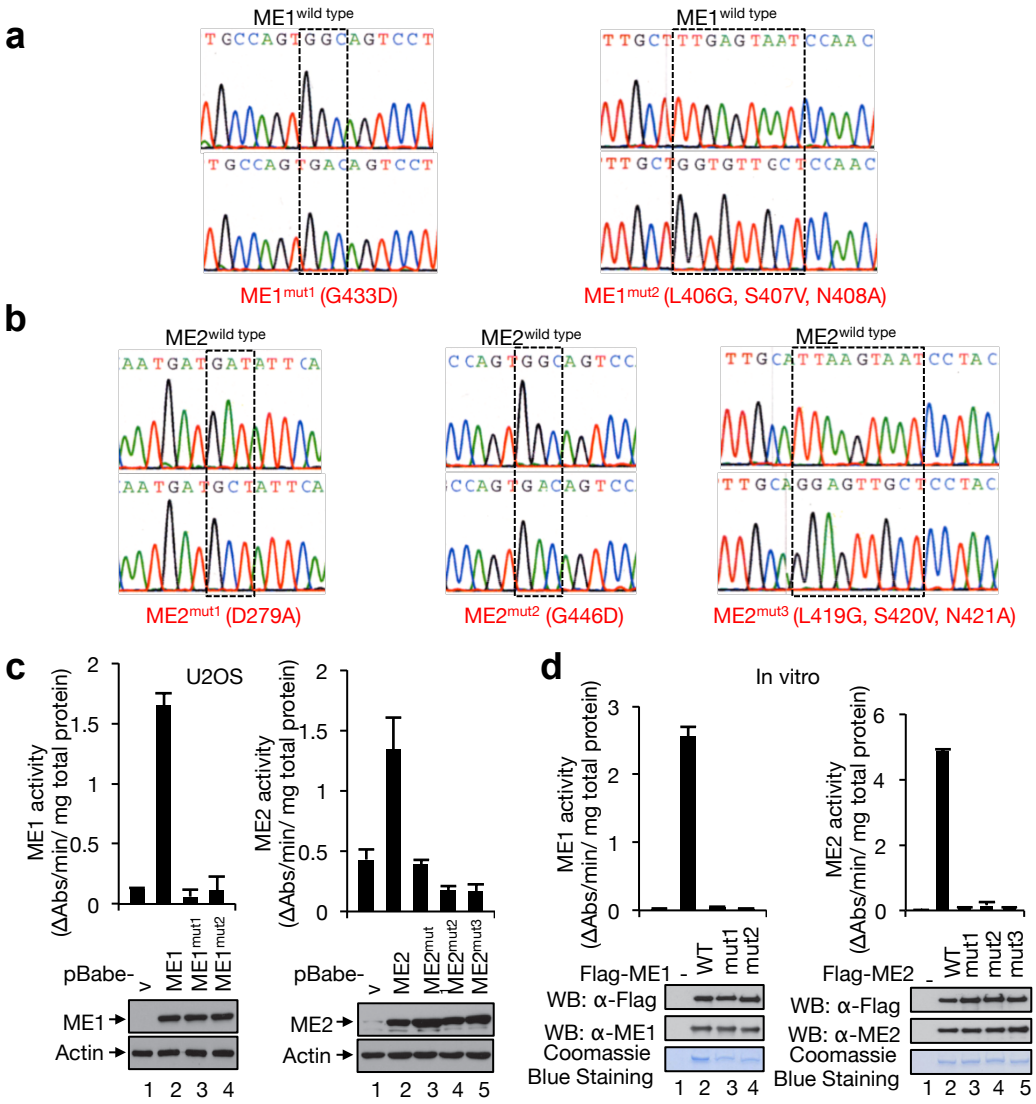

Supplementary Figure 6 | Generation of catalytically inactive ME mutants. a, b, Sequencing analysis of mutations in *ME1* (a) and *ME2* (b) genes. The choices of the amino acids to be mutated were based on structural and sequence information. **c**, U2OS cells were stably infected with control retroviruses or retroviruses expressing wild-type MEs or mutant MEs. ME activity in cell lysates (top; means ± SD, n=3) and protein expression (bottom) was assayed. **d**, Top: Activity of wild-type and mutant MEs in vitro (means ± SD, n=3). Bottom: Purified proteins were detected by Western blot using anti-Flag and anti-ME antibodies and by Coomassie blue staining.

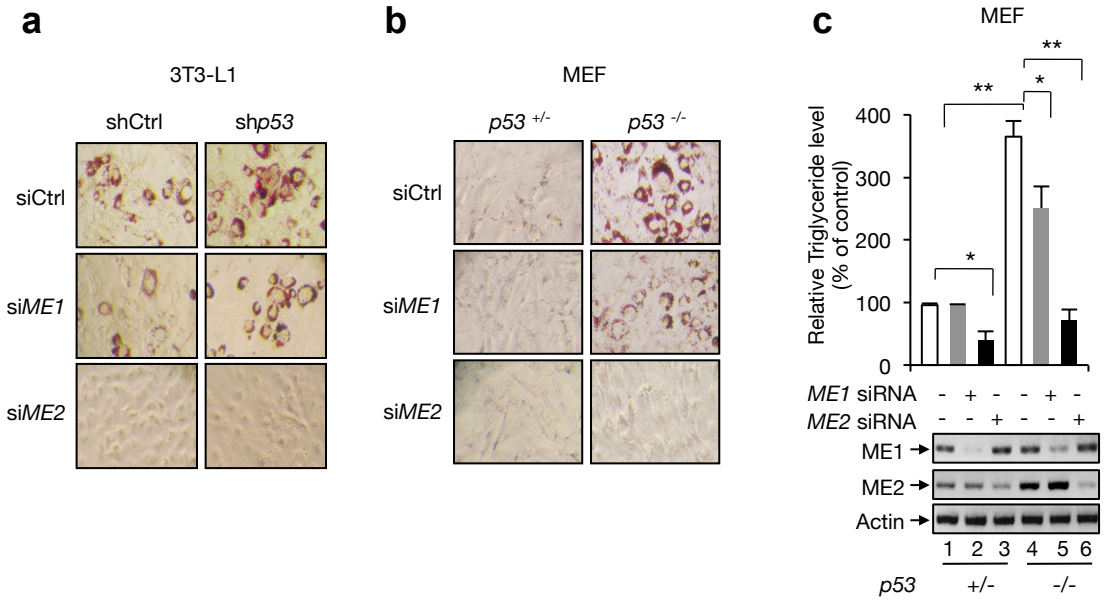

Supplementary Figure 7 | p53 regulates lipogenesis via ME1 and ME2. 3T3-L1 (a) and *p53*$^{+/-}$ and *p53*$^{-/-}$ MEF cells (b, c) were transfected with control, *ME1*, or *ME2* siRNA. Cells were cultured in the presence of insulin, rosiglitazone, isobutylmethylxanthine and dexamethasone. Total lipid (a, b) and triglyceride (means ± SD, n=3) (c, top) contents were analyzed. Gene expression was detected by RT-PCR (c, bottom).

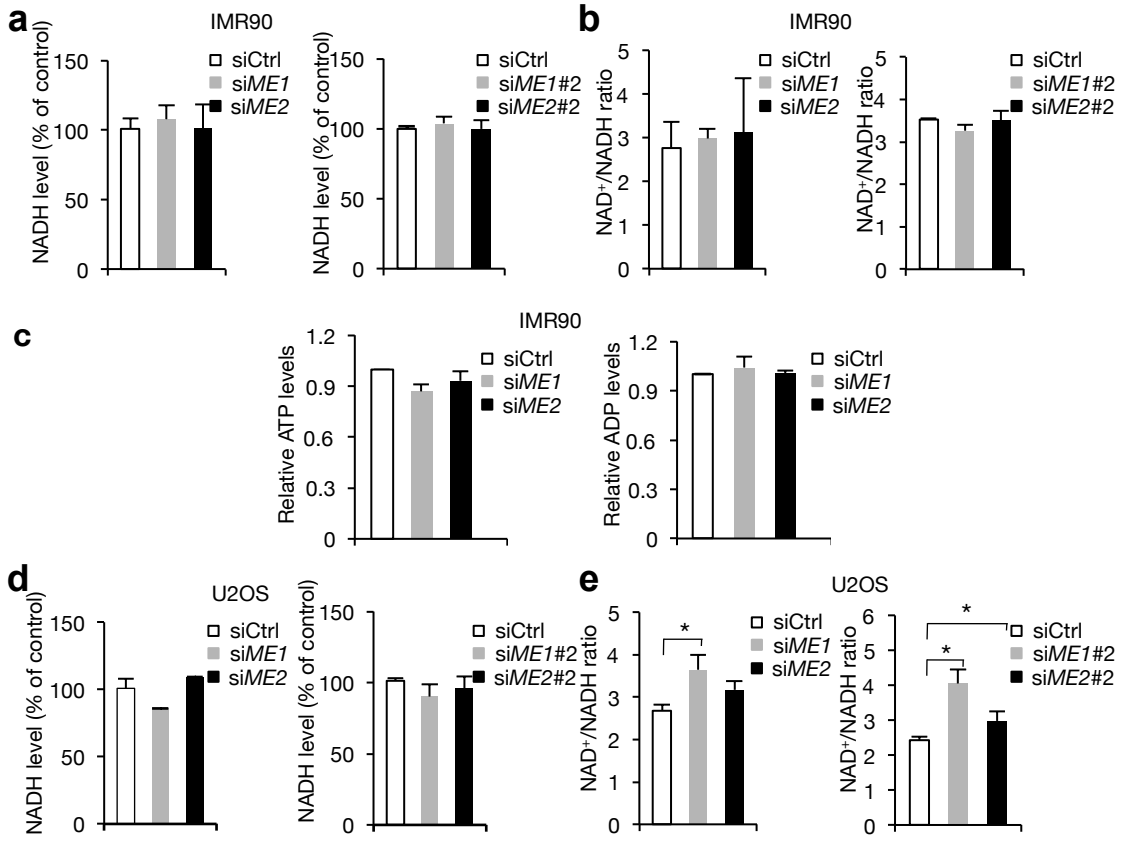

Supplementary Figure 8 | Effect of MEs on cellular levels of NADH and ATP. **a**, **d**, IMR90 (a) and U2OS (d) cells were transfected with different sets of *ME1* or *ME2* siRNA as indicated for 48 hours. NADH level was examined (mean ± SD, n=3). **c**, Relative ATP (left) and ADP levels (right) in IMR90 cells treated with *ME1*, *ME2*, or control siRNA (mean ± SD, n=3). **b**, **e**, IMR90 (b) and U2OS (e) cells were transfected with different sets of *ME1* or *ME2* siRNA as indicated for 48 hours, and NAD^+/NADH ratio was determined (mean ± SD, n=3).

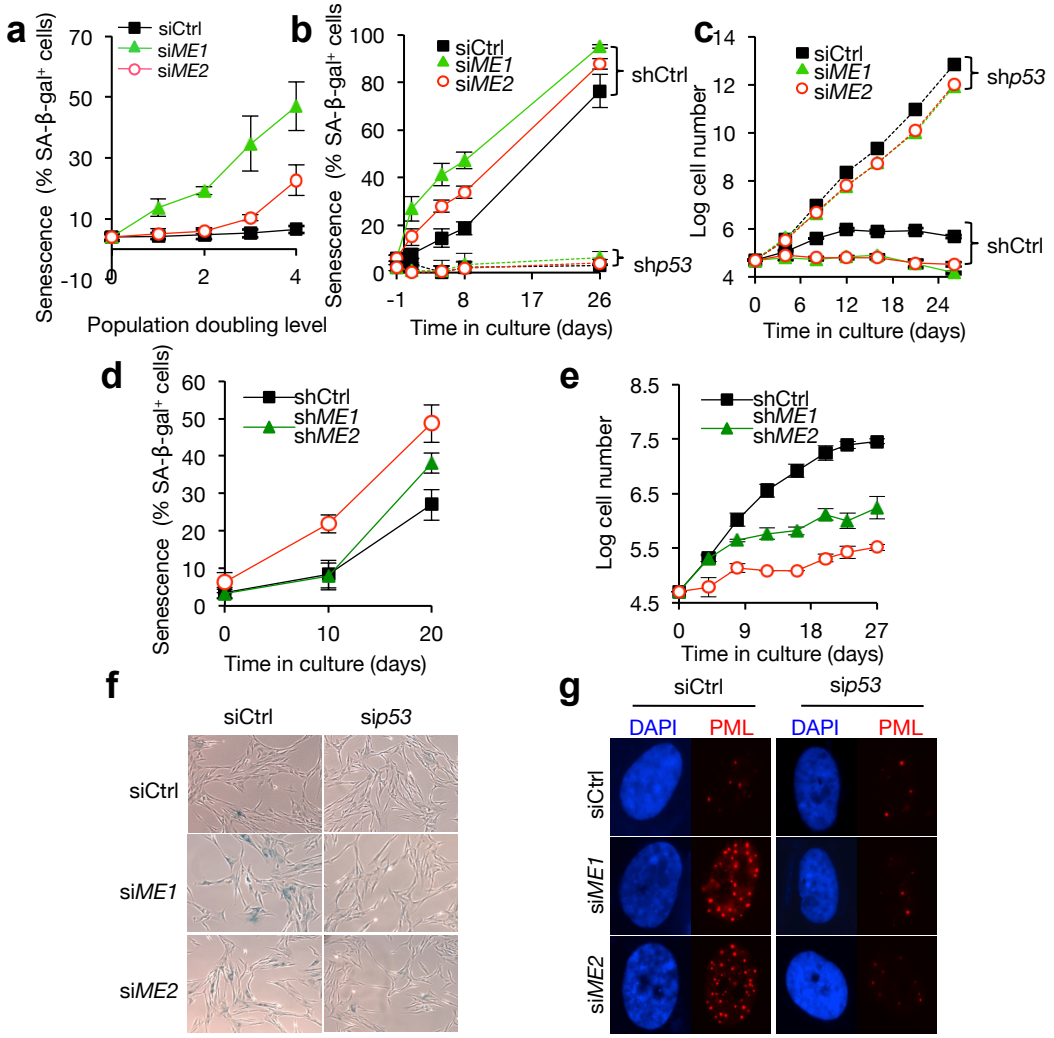

Supplementary Figure 9 | Down-regulation of ME1 or ME2 induces p53-mediated senescence in IMR90 cells. **a**, IMR90 cells transfected with control, *ME1*, or *ME2* siRNA were assayed for SA-β-gal expression. Data shown are average percentages of SA-β-gal-positive cells ± SD (n=3). **b**, **c**, IMR90 cells stably expressing *p53* shRNA or control shRNA were treated with control, *ME1*, or *ME2* siRNA as indicated. Percentages of SA-β-gal-positive cells (b) and replicative lifespans (c) (mean ± SD, n=3) are shown. **d**, **e**, IMR90 cells were stably infected with lentiviral vectors expressing *ME1*, *ME2*, or control shRNA. Percentages of SA-β-gal-positive cells (d) and replicative lifespans (e) (mean ± SD, n=3) are shown. **f**, **g,** IMR90 cells were transfected with control, *ME1*, *ME2*, and *p53* siRNA as indicated. Representative phase contrast images of SA-β-gal staining and morphology of IMR90 cells (f, related to Fig. 3b) and representative cells stained with anti-PML antibody and DAPI (g, related to Fig. 3c).

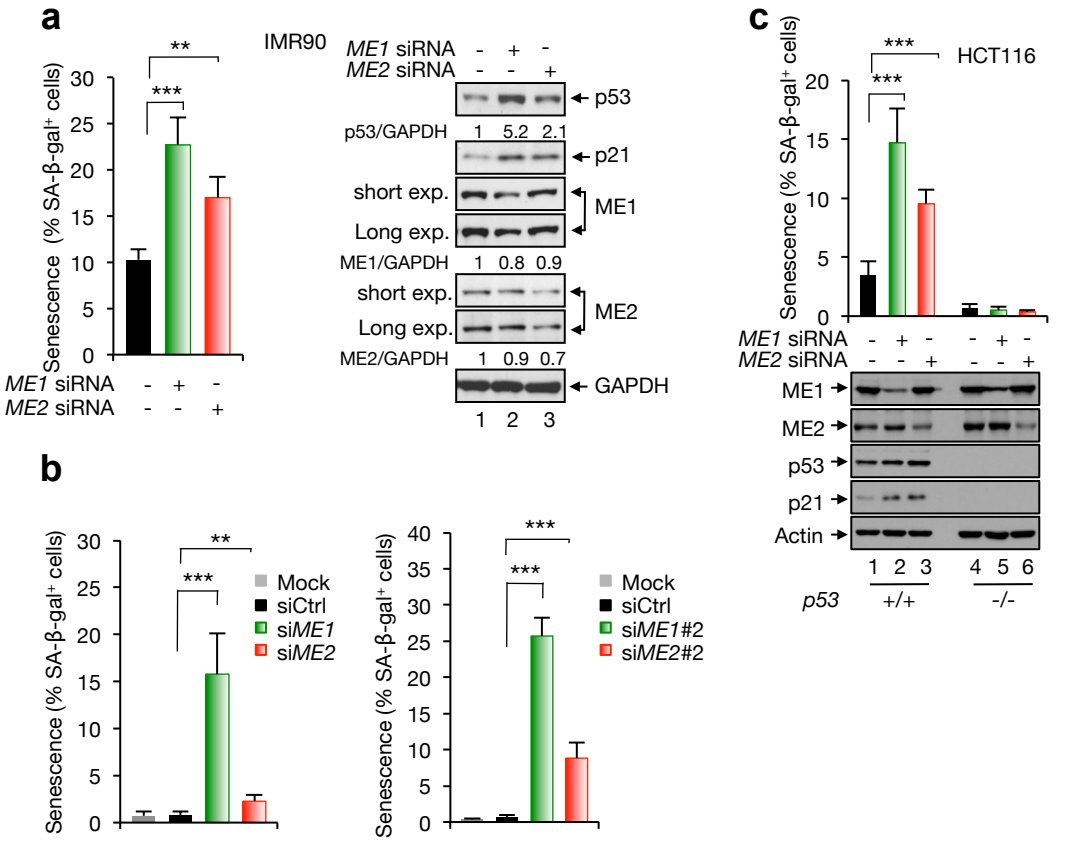

Supplementary Figure 10 | p53 activation and senescence induced by moderate ME knockdown in IMR90 cells and by ME knockdown in tumor cells. a, IMR90 cells were transfected with one-quarter of the amounts of *ME1*, *ME2*, or control siRNA used in the other experiments. Percentages of SA-β-gal-positive cells (left) and protein expression (right) are shown. **b**, Percentages of SA-β-gal positive cells (mean ± SD, n=3) in U2OS culture transfected with two different sets of siRNAs and cultured for 48 hr. Protein expression was shown in Supplementary Fig. 19b. **c,** $p53^{+/+}$ and $p53^{-/-}$ HCT116 cells transfected with control, *ME1*, or *ME2* siRNA and cultured for 72 h. Percentage of SA-β-gal positive cells (mean ± SD, n=3) are shown. Protein expression (bottom) are shown.

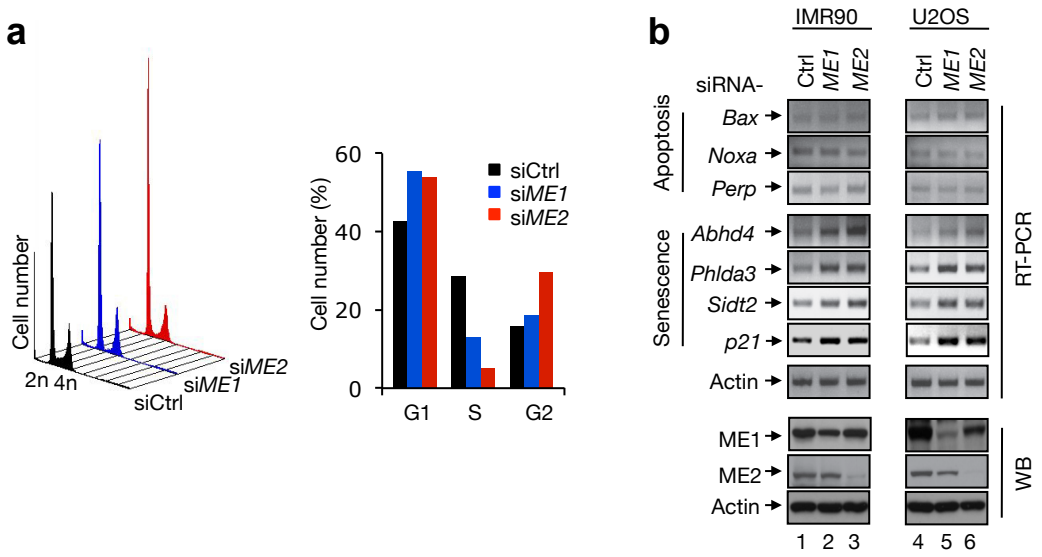

Supplementary Figure 11 | ME down-regulation induces senescence but not apoptosis. **a,** Knockdown of *ME*s in IMR90 cells leads to cell cycle arrest but not apoptosis. IMR90 cells were transfected with *ME1*, *ME2*, or control siRNA for 48 h. Left: Cell cycle distribution determined by flow cytometry. Right: percentages of cells in the G1, S, and G2 phases of the cell cycle (right). **b,** Knockdown of MEs specifically increases the expression of senescence-associated genes. IMR90 cells and U2OS cells were transfected with *ME1*, *ME2*, or control siRNA for 48 h. Expression of senescence- and apoptosis-associated genes was examined by using RT-PCR. The expression of ME1 or ME2 was determined by Western blot.

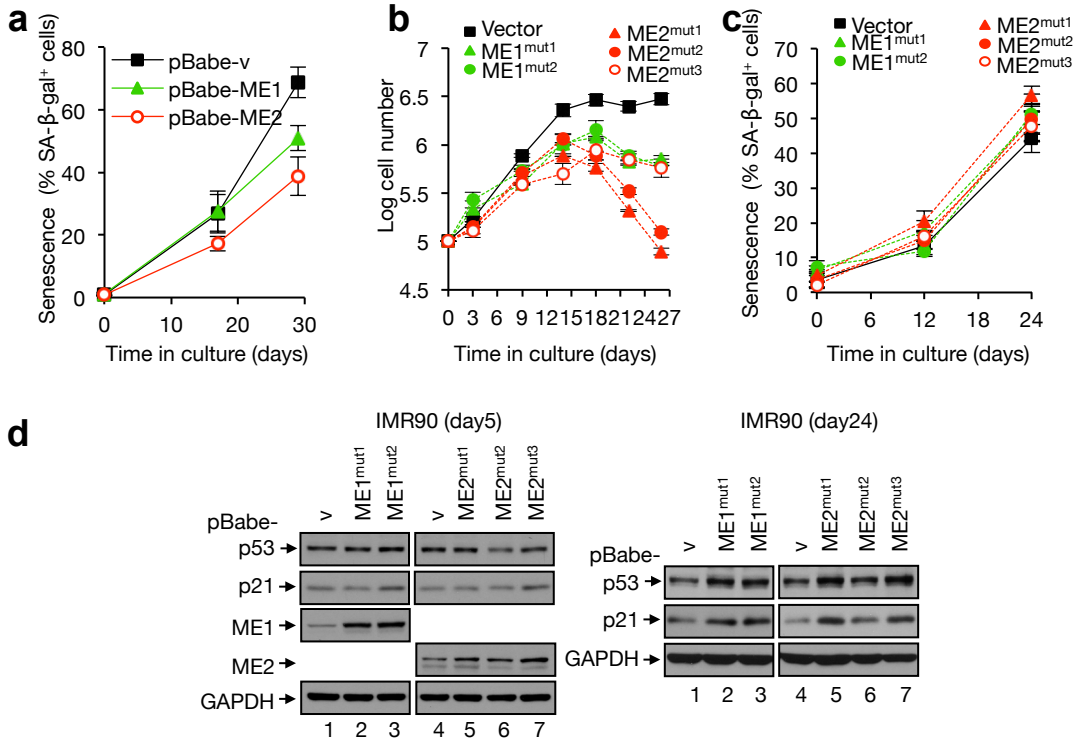

Supplementary Figure 12 | Wild-type, but not mutant, MEs suppress p53 activation and senescence. a, IMR90 cells stably infected with retroviral vectors expressing ME1, ME2, or control vector were cultured for different days and assayed for senescent phenotypes. Results are mean ± SD of a representative experiment done in triplicate. **b**, Replicative lifespan of IMR90 cells stably infected with retroviral vectors expressing mutant MEs or control vector (mean ± SD, n=3). Arrows indicate the onset of senescence. **c**, SA-β-gal activity in IMR90 cells stably expressing mutant MEs or vector control at different days. **d**, IMR90 cells stably expressing mutant ME1, mutant ME2, or empty vector were cultured for 5 (left) or 24 (right) days. Protein expression was analyzed by Western blot.

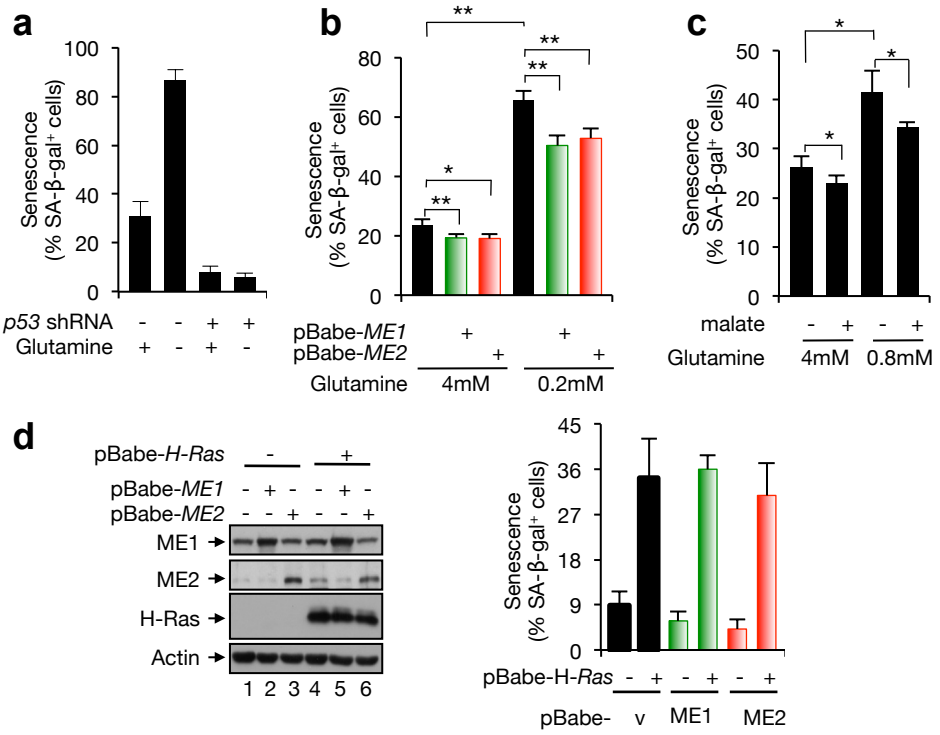

Supplementary Figure 13 | Role of MEs in senescence induced by glutamine withdrawal or oncogenic Ras. a, IMR90 cells stably expressing *p53* shRNA or control shRNA were cultured in medium with or without glutamine for 72 h. Percentages of senescent cells (means ± SD, n=3) are shown. **b**, IMR90 cells stably expressing ME1, ME2, or empty vector were cultured in medium with 4 mM or 0.8 mM glutamine for 72 h. Percentages of senescent cells (means ± SD, n=3) are shown. **c**, IMR90 cells were cultured in medium with 4 mM or 0.8 mM glutamine. After 24 h, 1 mM malate was added into the medium, and cells were cultured for another 48 h. Percentages of senescent cells (means ± SD, n=3) are shown. **d**, IMR90 cells stably expressing MEs or vector control were further infected with retroviral vectors expressing H-Ras^{V12} as indicated. Shown are protein expression (left) and % SA-β-gal-positive cells (mean ± SD, n=3; right). **P*<0.05, ***P*<0.01.

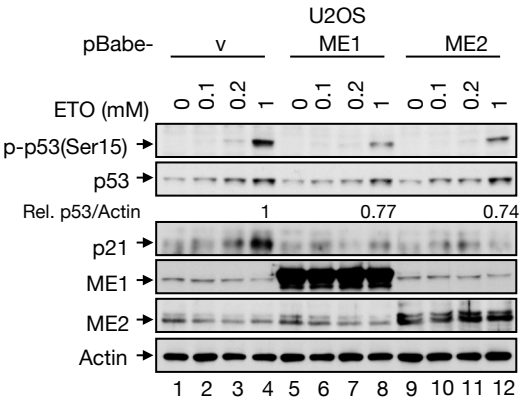

Supplementary Figure 14 | ME1 and ME2 inhibit p53 activation upon DNA damage. U2OS cells stably expressing ME1 or ME2 and control U2OS cells were treated with increasing amounts of ETO for 24 h. Cell lysates were analyzed by Western blot.

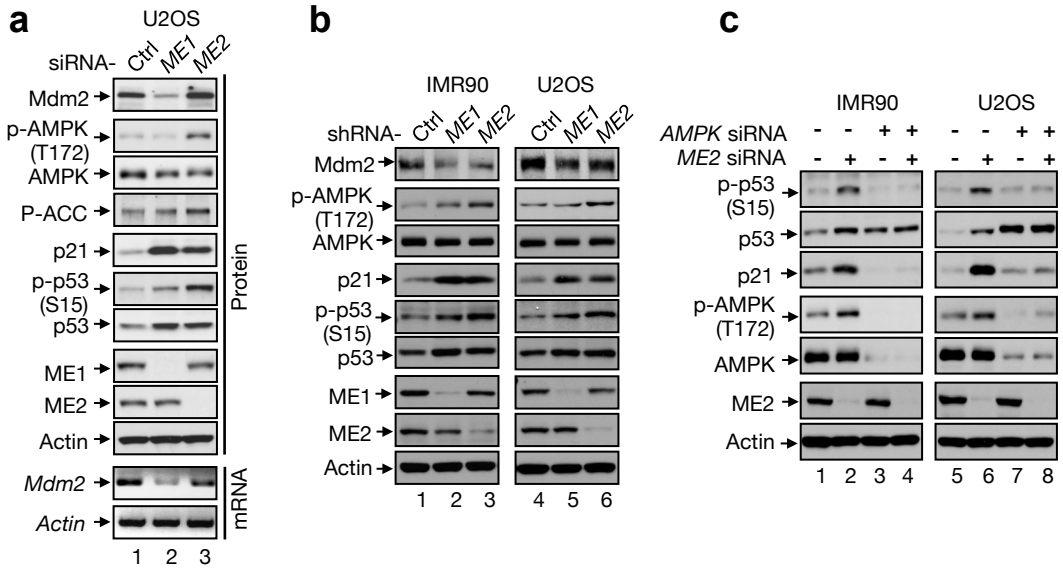

Supplementary Figure 15 | ME1 and ME2 down-regulation activates p53 via Mdm2 and AMPK, respectively. a, U2OS cells were transfected with control, *ME1* or *ME2* siRNA. Protein expression and the activation of p53 and AMPK were examined by Western blot. ACC: Acetyl-CoA carboxylase. **b**, IMR90 (left) and U2OS (right) cells were infected with lentiviral vectors expressing *ME1*, *ME2*, or control shRNA. Protein expression and the activation of p53 and AMPK were examined by Western blot. mRNA transcript was detected by RT-PCR. **c**, IMR90 (left) and U2OS (right) cells were transfected with control, *ME2*, and *AMPK* siRNAs in the indicated combination. Cell lysates were analyzed by Western blot.

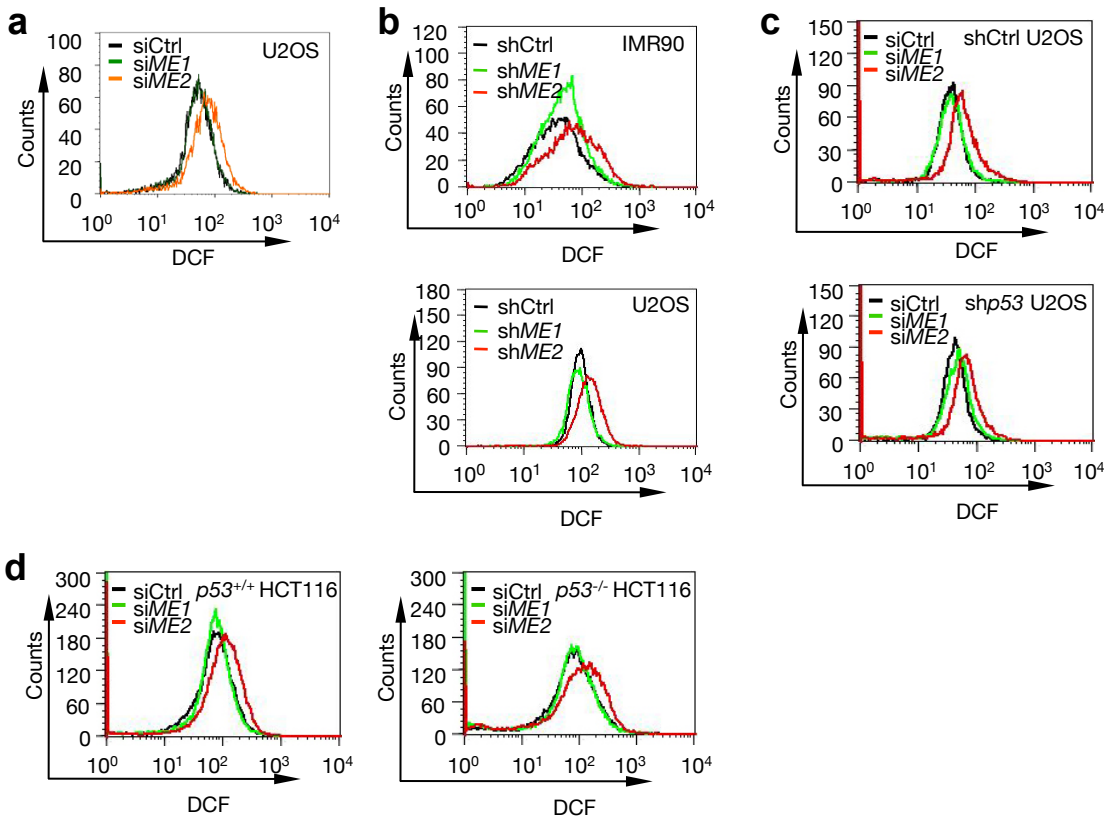

Supplementary Figure 16 | ME2 down-regulation elevates cellular ROS levels independent of p53. **a**, U2OS cells were transfected with *ME1*, *ME2* or control siRNA. ROS was measured by 2′,7′-di-chlorofluorescein (DCF) staining and flow cytometry. **b,** ROS levels in IMR90 (top) and U2OS (bottom) cells stably expressing *ME1*, *ME2* or control shRNA. **c**, **d,** U2OS cells stably infected with lentiviral vectors expressing *p53*-specific shRNA or control shRNA (c) and $p53^{+/+}$ and $p53^{-/-}$ HCT116 cells (d) were transfected with control, *ME1*, or *ME2* siRNA. ROS were measured.

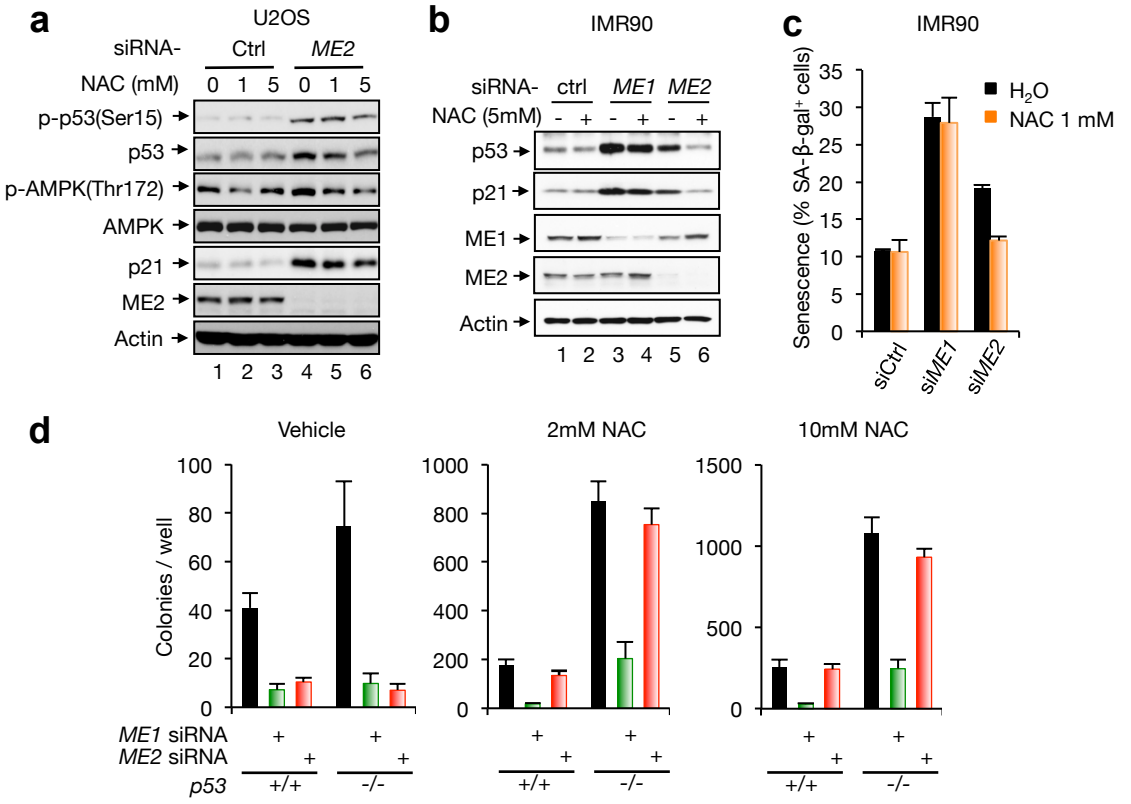

Supplementary Figure 17 | ME2 down-regulation activates AMPK and p53 and induces senescence due to an increase in ROS. a, U2OS cells transfected with control siRNA or *ME2* siRNA were treated with increased amount of NAC for 72 h. Cell lysates were analyzed by Western blot. **b**, IMR90 cells transfected with control, *ME1*, or *ME2* siRNA were cultured in presence or absence of 5 mM NAC for 72 h. Cell lysates were analyzed by Western blot. **c**, IMR90 cells transfected with control, *ME1* or *ME2* siRNA were treated with increasing amount of NAC as indicated for 48 h and cell senescence was determined (means ± SD, n=3). **d**, $p53^{+/+}$ and $p53^{-/-}$ HCT116 cells transfected with *ME1*, *ME2* or control siRNA were plated in culture medium containing increasing amounts of NAC or vehicle control in soft agar and cultured for 2 weeks. Numbers of colonies with a diameter greater than 20 µm were quantified (mean ± SD, n=3).

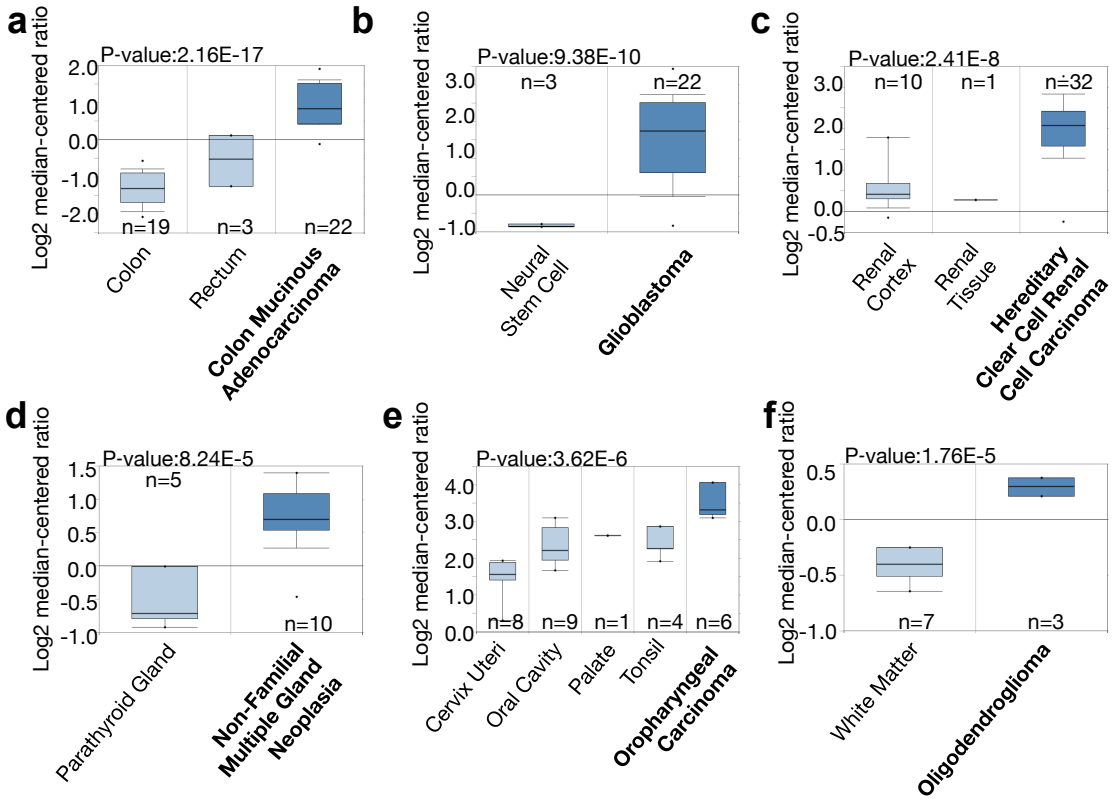

Supplementary Figure 18 | Up-regulation of *ME1* and *ME2* mRNAs in human tumors. a-c, Box plot comparing *ME1* transcript levels in colon adenocarcinoma (a) (http://tcga-data.nci.nih.gov/tcga), glioblastoma (b)[34], renal cell carcinoma (c)[35], and their normal counterparts. **d-f**, *ME2* mRNA expression in neoplasia human parathyroid samples (d)[36]. oropharyngeal carcinoma (e)[37], and oligodendroglioma white matter (f)[38] samples were compared with the corresponding normal tissues. The graphs were derived from published data available through the ONCOMINE database. The differential gene expression data are centered on the median of expression levels and plotted on a log2 scale. The *P* value was calculated using a two-sample t test. Whiskers indicate minimum and maximum data values that are not outliers. The number of samples (n) in each class is indicated.

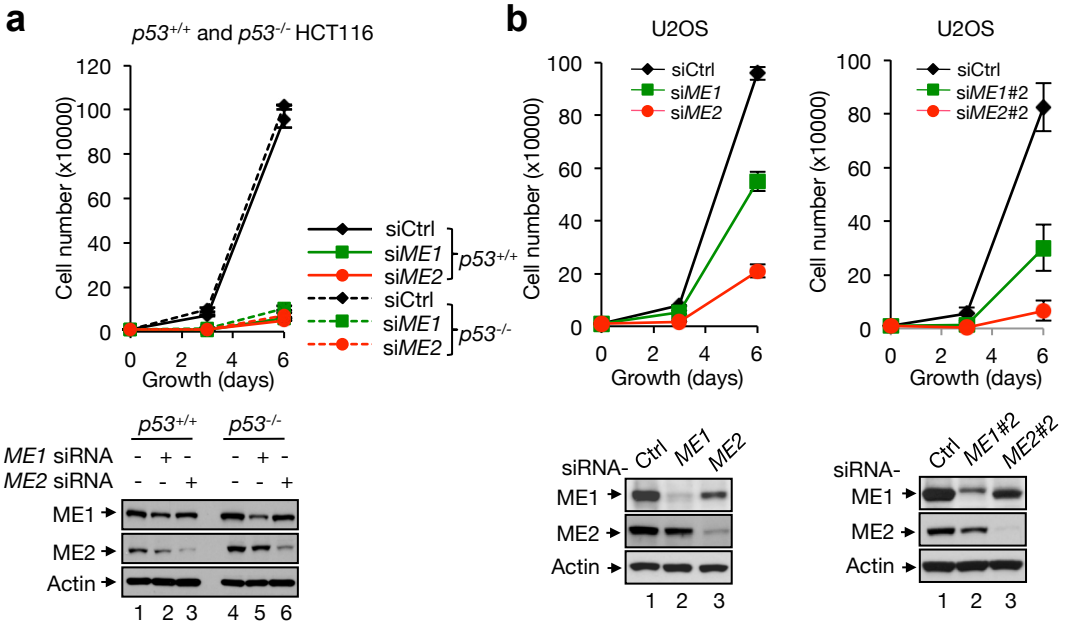

Supplementary Figure 19 | Silencing ME expression severely impairs tumor cell growth. a, $p53^{+/+}$ and $p53^{-/-}$ HCT116 cells were transfected with control, *ME1*, or *ME2* siRNA. Cell growth and protein expression are shown. **b**, Growth of U2OS cells transfected with control or two different sets of siRNAs targeting *ME1* or *ME2* as indicated. Data are means ± SD (n=3). Protein expression is shown below.

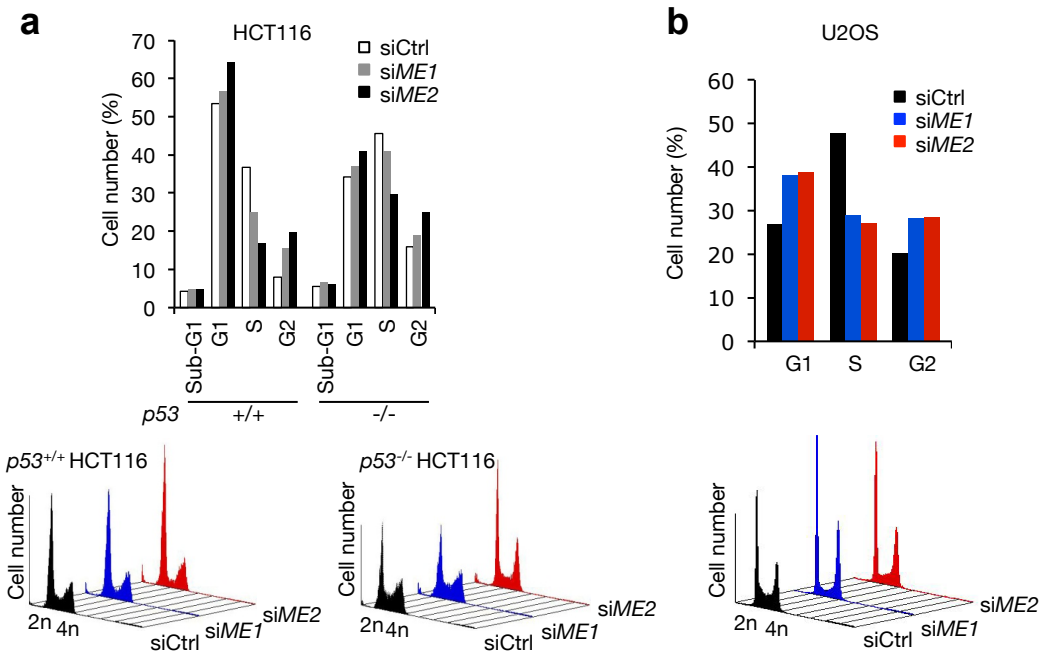

Supplementary Figure 20 | Knockdown of either ME1 or ME2 leads to cell cycle arrest in HCT116 cells and U2OS cells. *p53*$^{+/+}$ and*d p53*$^{-/-}$ HCT116 cells (a) and U2OS cells (b) were treated with *ME1*, *ME2*, or control siRNA for 48 h. Bottom: Cell-cycle distribution measured by flow cytometry after propidium iodide-stained (bottom). Top: Percentages of cells in the G1, S, and G2 phase of the cell cycle.

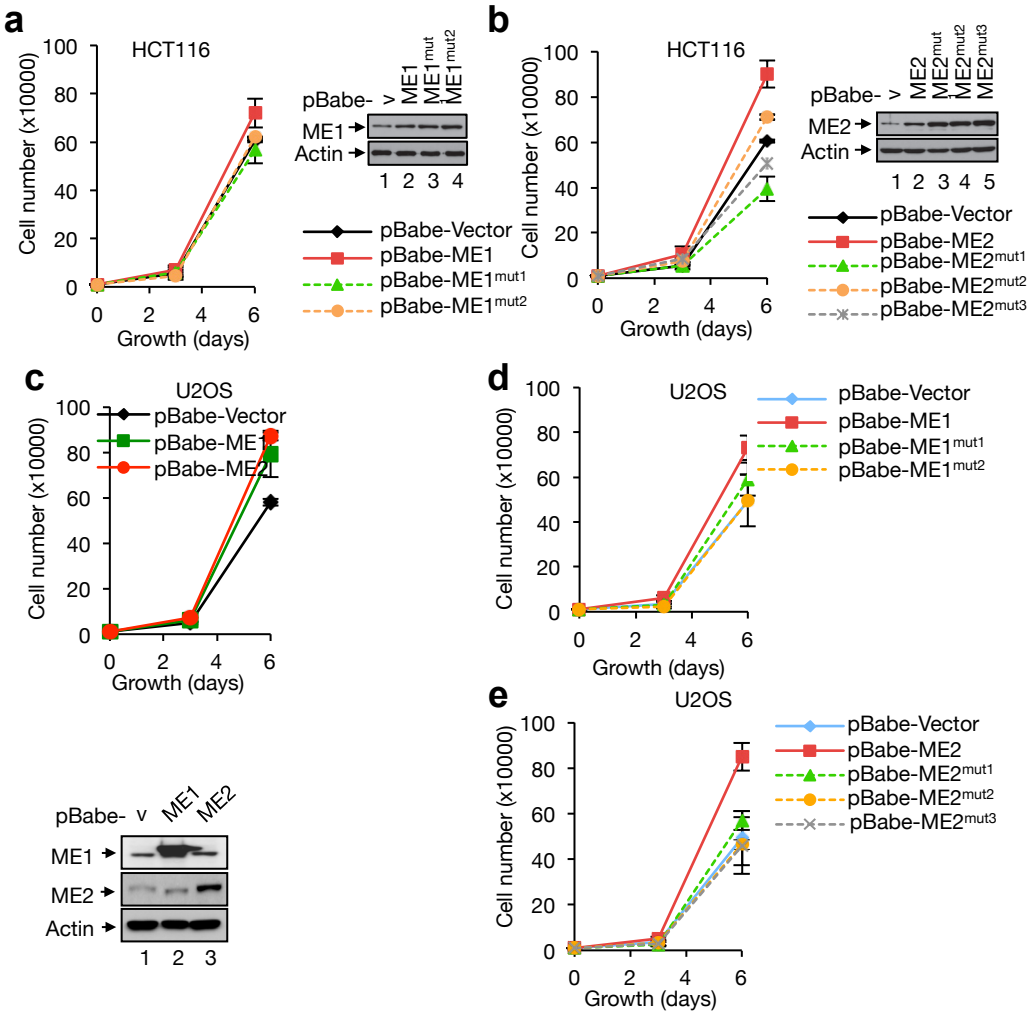

Supplementary Figure 21 | Wild-type, but not mutant, MEs enhances cell growth. **a**, **b**, Growth of *p53*$^{+/+}$ HCT116 cells stably infected with retroviruses expressing wild-type ME1 or each of the mutant ME1s (a), or with retroviruses expressing wild-type ME2 or each of the mutant ME2s (b), or control viruses (a, b). Data are means ± SD (n=3). **c**, Growth (means ± SD, n=3) of U2OS cells stably infected with retroviruses expressing ME1, ME2, or control viruses. Protein expression is shown below.
d, **e**, Growth (means ± SD, n=3) of U2OS cells infected with the indicated retroviruses.

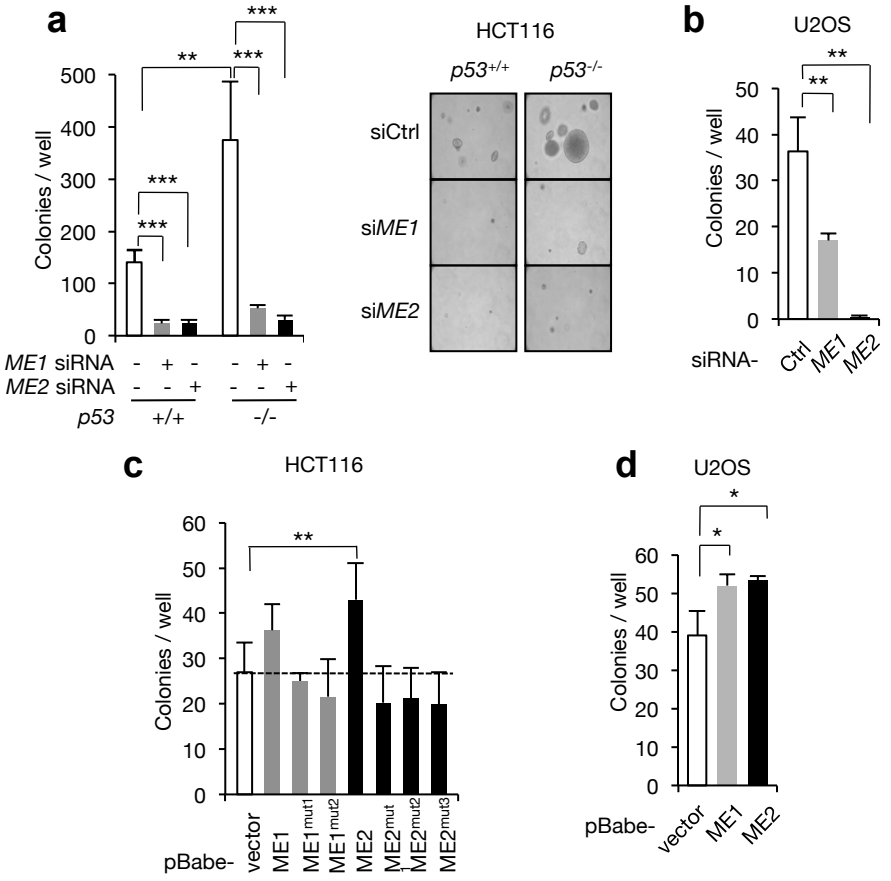

Supplementary Figure 22 | Essential role of MEs in anchorage-independent growth. **a**, *p53*$^{+/+}$ *and p53*$^{-/-}$ HCT116 cells transfected with *ME1*, *ME2*, or control siRNA were plated in culture medium in soft agar and cultured for 2 weeks. Left: Numbers of colonies with a diameter greater than 20 μm were quantified (mean ± SD, n=3). Right: Representative images of colonies in soft agar. **b**, Colony-formation assay of U2OS cells transfected with control siRNA, *ME* siRNA, or *ME2* siRNA. Data are means ± SD (n=3). **c**, HCT116 cells stably infected with retroviruses containing wild-type MEs or mutant MEs or control viruses (vector) were plated in culture medium in soft agar and cultured for 2 weeks. Numbers of colonies with a diameter greater than 20 μm were quantified (mean ± SD, n=3). **d**, Colony-formation assay of U2OS cells stably infected with retroviruses expressing ME1 or ME2 or control viruses. Data are means ± SD (n=3). **P*<0.05, ***P*<0.01, ****P*<0.001.

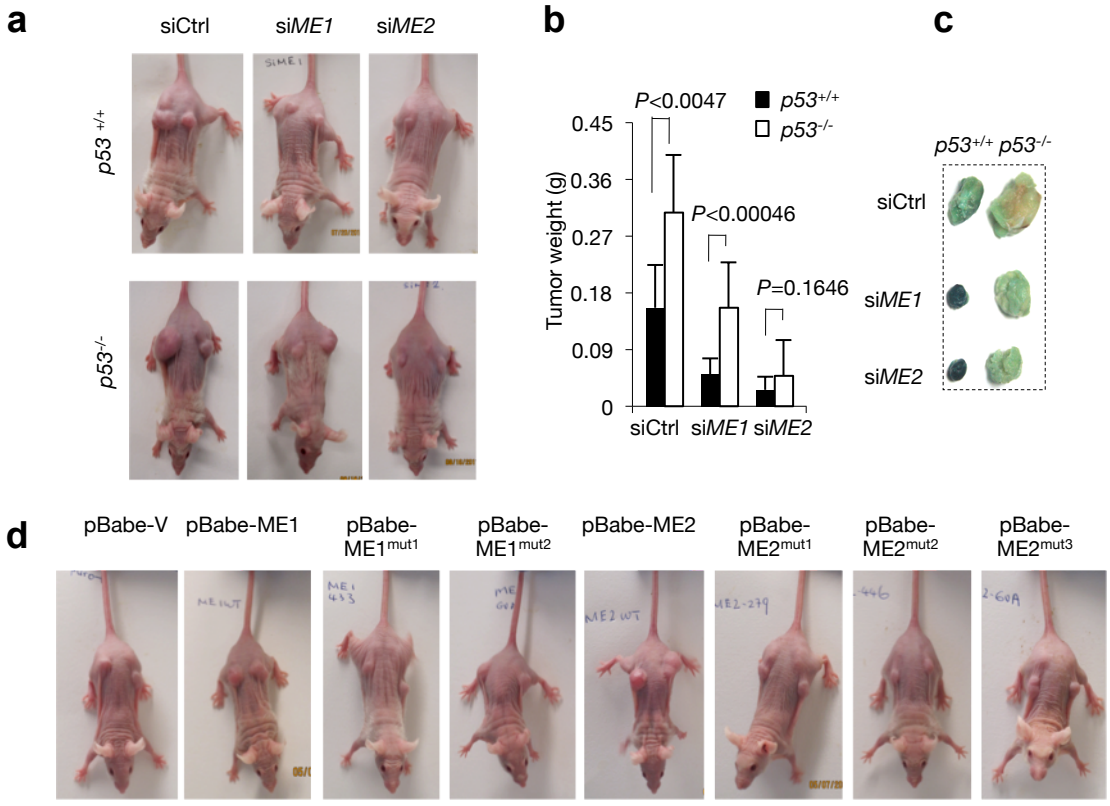

Supplementary Figure 23 | A role of MEs in the growth of *p53*$^{+/+}$ and *p53*$^{-/-}$ tumors. **a**, *p53*$^{+/+}$ *and p53*$^{-/-}$ HCT116 cells transfected with *ME1*, *ME2*, or control siRNA were injected in nude mice separately. Mice were analyzed two weeks later for tumor formation. Representative images of the mice are shown. Related to Fig. 4e. **b**, Comparison of the tumor growth in a *p53*$^{+/+}$ versus *p53*$^{-/-}$ background (means ± SD, n=6). Related to Fig. 4e. **c**, Tumors from (**a**) were stained for SA-β-gal expression. **d**, *p53*$^{+/+}$ HCT116 cells stably infected with retroviruses containing wild-type MEs, mutant MEs, or control viruses were injected in nude mice separately. Representative images of the mice are shown. Related to Fig. 4f.

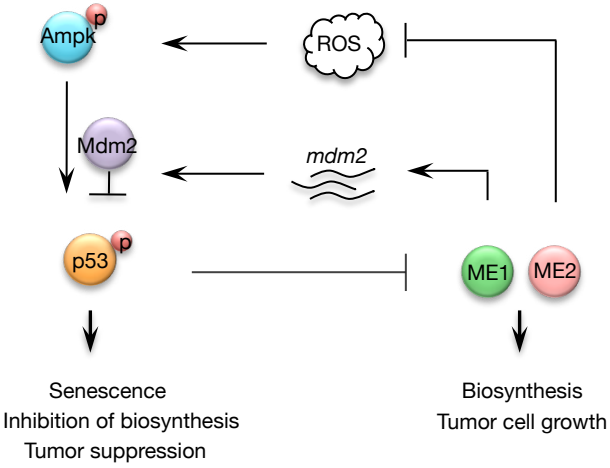

Supplementary Figure 24 | A model for the p53-MEs pathway in metabolism, senescence, and tumor growth.

Figure 1a

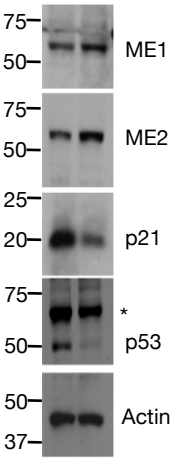

Figure1e

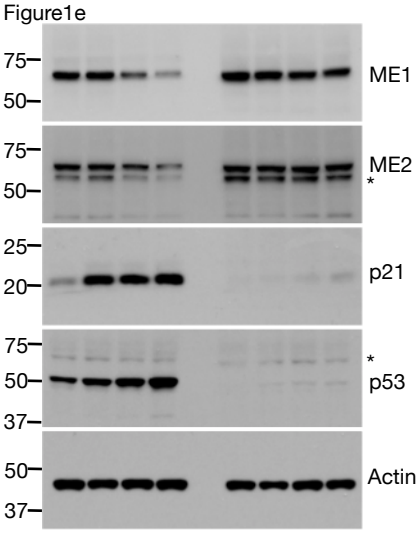

Figure 2a

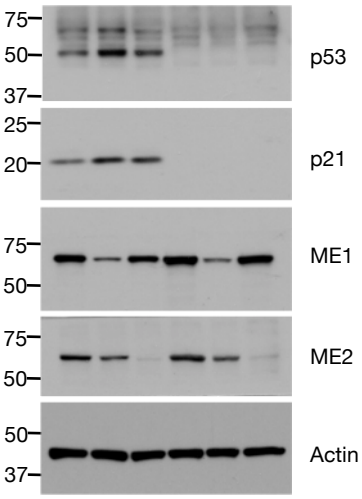

Figure 2b

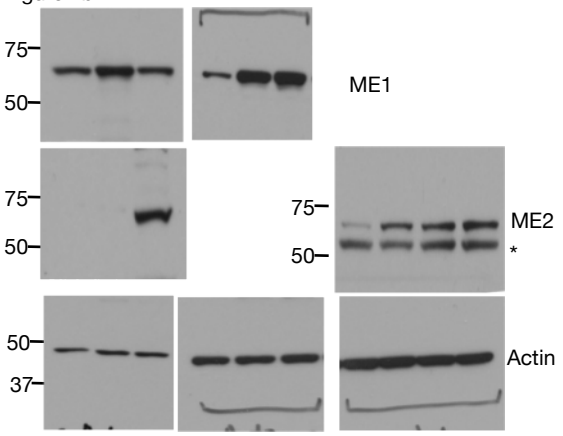

Figure 2e

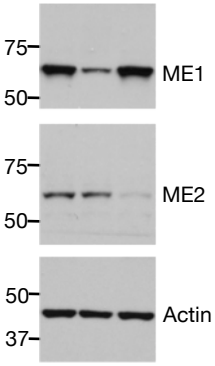

Figure 3d

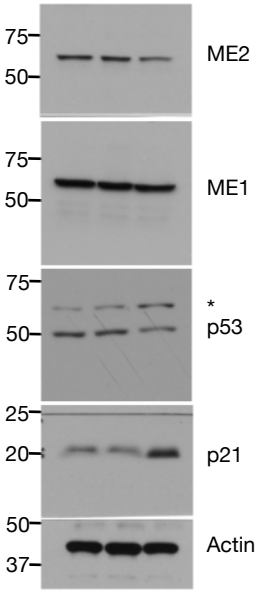

Figure 2d

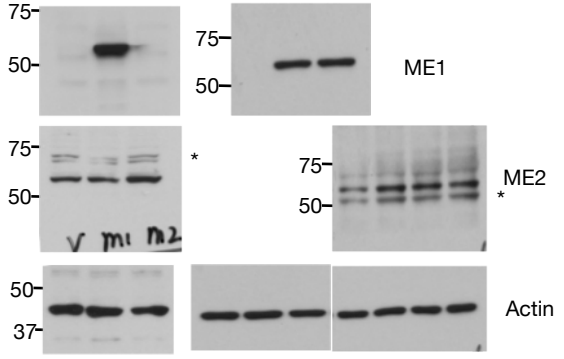

Figure 2f

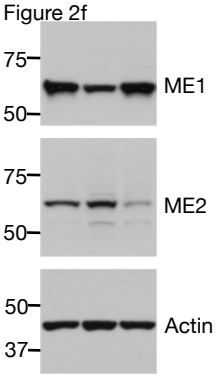

Figure 3f

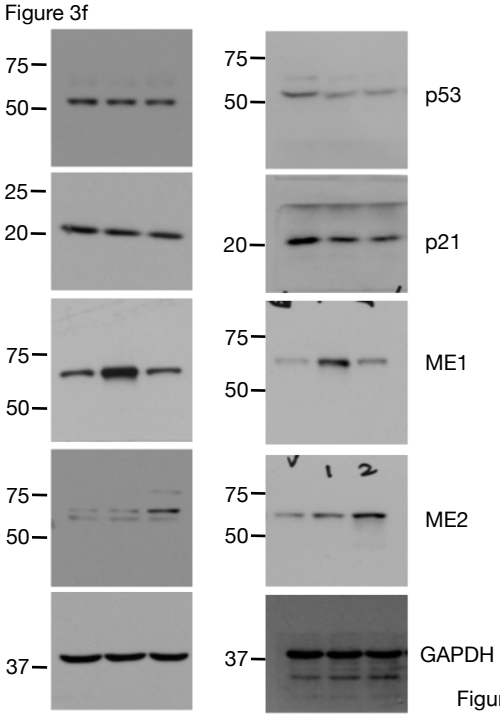

Figure 4a

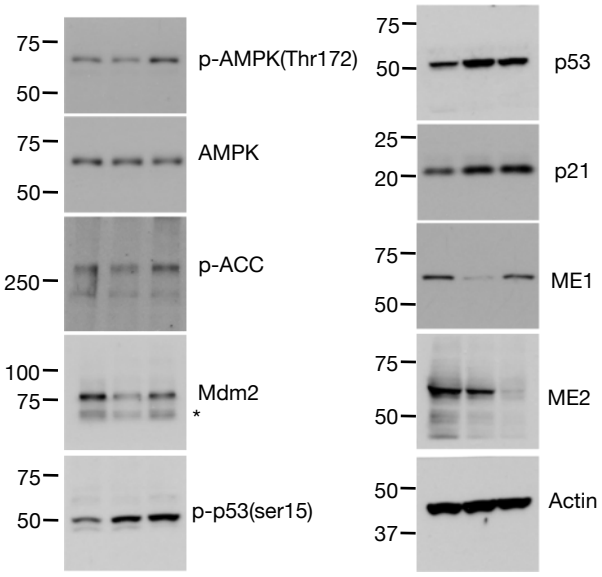

Figure 4b

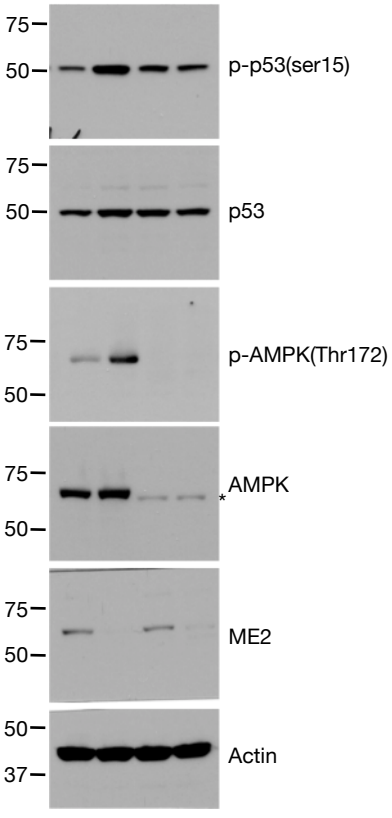

Figure 4d

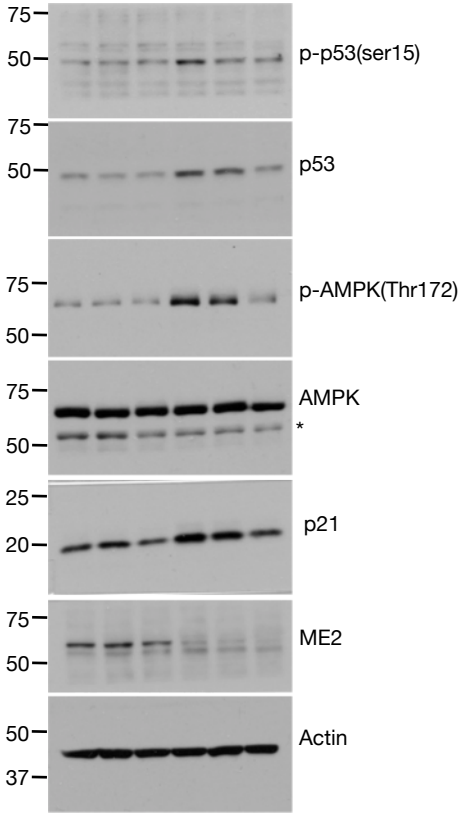

Supplementary Figure 25| Full scans of western data. *Non-specific bands

Additional References

34 Lee, J. et al. Tumor stem cells derived from glioblastomas cultured in bFGF and EGF more
closely mirror the phenotype and genotype of primary tumors than do serum-cultured cell lines. *Cancer Cell* **9**, 391-403 (2006).
35 Beroukhim, R. et al. Patterns of gene expression and copy-number alterations in von-hippel lindau disease-associated and sporadic clear cell carcinoma of the kidney. *Cancer Res* **69**, 4674-4681 (2009).
36 Morrison, C. et al. Molecular classification of parathyroid neoplasia by gene expression profiling. *Am J Pathol* **165**, 565-576 (2004).
37 Pyeon, D. et al. Fundamental differences in cell cycle deregulation in human papillomavirus-positive and human papillomavirus-negative head/neck and cervical cancers. *Cancer Res* **67**, 4605-4619 (2007).
38 Shai, R. et al. Gene expression profiling identifies molecular subtypes of gliomas. *Oncogene* **22**, 4918-4923 (2003).